CONTINUOUS AND LABEL-FREE MICROFLUIDIC CELL SEPARATION

T. M. Geislinger, B. Eggart, S. Braunmüller, L. Schmid, and T. Franke*

Soft Matter and Biological Physics Group

EPI, University of Augsburg, GERMANY

ABSTRACT

Using size and deformability as intrinsic biomarkers, we separate red blood cells (RBC) from other blood components based on the non-inertial lift effect. We exploit this purely viscous, repulsive cell-wall interaction at low Reynolds numbers to induce a lateral migration of soft objects perpendicular to the streamlines of the fluid which closely follows theoretical prediction by Olla [1]. We demonstrate the separation of RBCs, blood platelets, solid microspheres, and circulating MV3-melanoma cells and study the influence of the flow rate on the separation. The method can be used for passive, continuous and label-free cell classification in on-chip blood analysis.

KEYWORDS: red blood cells, blood platelets, non-inertial lift, cell separation, microfluidics

INTRODUCTION

An important task for microfluidic examination of blood is continuous and label-free cell classification and sorting. Multiple methods are available and summarized in several reviews [2-4]. We demonstrate a simple microfluidic device for the separation of soft objects by size and deformability using the non-inertial hydrodynamic lift effect. The non-inertial lift is a purely viscous effect in low velocity flow fields. The process is passive, continuous and label-free and operates at gentle shear forces. We find our experiments to be in excellent agreement with theoretical prediction [1].

THEORY

The non-inertial lift provides the general background for the analysis of our experiments. At low Reynolds number Re, this cell-wall interaction is the dominant hydrodynamic effect to induce cross-streamline migration of deformable objects in shear flow [5;6]. In the regime of low Re, also called the Stokes regime [7] the flow field is laminar and reversible in time. There exist several possibilities to break this highly symmetric condition such as the deformation of soft objects due to flow stresses, shear flow in the vicinity of a wall, Poiseuille flow or interactions between the suspended objects [7-9]. The break of the symmetry results in a cross-streamline migration of the objects which is generally directed away from the wall and, in Poiseuille flow, directed towards the centerline of the flow field [7;8;10]. For RBCs in blood flow, this migration is known as the Fåhræus-Lindqvist effect [11], leading to a reduction of the apparent viscosity [9] and to the margination phenomenon for leukocytes and blood platelets[12].

The non-inertial lift has been examined from a theoretical point of view by several groups [1;7;10]. One expression for the lateral lift velocity $v_l(z)$ derived by Olla [1] yields:

$$v_l(z) = \frac{\dot{\gamma}(z) \cdot R^3 \cdot U(\lambda, r_1, r_2)}{z^2} \qquad (1)$$

Here, the lift velocity depends on the shear rate $\dot{\gamma}$, the effective radius of the object $R = (a_1 a_2 a_3)^{1/3}$, with the elliptical semi-axes of the object, a_1, a_2 and a_3 and the distance z between the center of mass of the object and the wall for $z \gg R$. For smaller distances to the wall ($z \approx R$) other descriptions of the lift velocity have to be taken into account (3; 13). The quantity $U(\lambda, r_1, r_2)$ is a dimensionless drift velocity that depends on the viscosity contrast $\lambda = \eta_{in} / \eta_{out}$ of the internal and external fluid and the geometry of the object described by $r_1 = a_1/a_3$ and $r_2 = a_2/a_3$. For spherical particles, $U(\lambda, r_1, r_2) = 0$ and the non-inertial lift vanishes. For a fixed shape, $U(\lambda, r_1, r_2)$ decreases with increasing viscosity ratio λ [1]. This prediction has been shown to be in qualitative agreement with experiments and theoretical results for deformable lipid vesicles in microgravity [14] and for RBCs and blood platelets in Poiseuille flow [15]. To compare our experimental results for RBCs, blood platelets and microspheres with the theoretical prediction we use the object properties summarized in [15] and numerically calculate the adopted height at the end of the channel with the downstream velocity defined by a simplified Poiseuille-flow profile.

EXPERIMENTAL

We prepare a PBS-dextran (MW: 400 kDa – 500 kDa, Sigma Aldrich Inc.) solutions of *5% w/w* with a viscosity of $\eta_{out} = 7mPas$ and a density $\rho_{7mPas} = 1.03\ g/cm^3$ for the experiments. For the sheath flow the pure PBS-dextran solution is drawn into a Hamilton gastight syringe. To prepare the sample solutions, blood is drawn from healthy voluntary donors and anticoagulated with ethylenediaminetetraacetic acid (EDTA). We wash the blood three times in isoosmotic phosphate buffered saline (PBS) of *pH = 7.4* and partly withdraw blood plasma and RBCs after each centrifugation step. The solution then contains a two to three times higher concentration of blood platelets compared to whole blood and the hematocrit is $Hct \approx 1\%$. We further dilute the sample 1:10 with the PBS-dextran mixture to a final hematocrit of $Hct \approx 0.1\%$ and transfer it into another Hamilton gastight syringe. For the experiments on the separation of RBCs and melanoma cells, we wash the blood three times and completely remove blood plasma and the buffy coat. The solid microspheres we use are polystyrene beads with a diameter of 3 µm (Polybeads, Polysciences Inc.). We use MV3-

melanoma cells (obtained from S. Schneider, University Medical Center Münster) as representative cell line for aggressive circulating tumor cells. The cells are maintained in MEM medium (Biochrom AG) supplemented with 10% fetal bovine serum (Biochrom AG) and 1% penicillin (Biochrom AG). For the experiments, confluent cells are harvested with Trypsin/EDTA (Biochrom AG) and diluted in the PBS-dextran solution with *5 mg/ml* EDTA and *2 mg/ml* bovine serum albumin (BSA).

Our microdevice consists of a simple single-layer polydimethylsiloxane (PDMS) microchannel that is fabricated by standard soft lithography. Its geometry is illustrated in *Figure 1*. Cells are injected into the device through a rectangular inlet channel with a cross-section of *(110 x 30) µm* in *y* and *z* direction as denoted in *Figure 1* and are hydrodynamically focused by a sheath flow. The sheath flow inlet and the adjacent main channel have a square cross-section of *(110 x 110) µm* in *y* and *z* direction. The distance between the measurement positions x_1 at the inlet and x_2 near the end of the channel is *(19 ± 0.5) mm*. The microfluidic device is mounted on a Zeiss Axiovert 200m inverted video microscope equipped with a Photron Fastcam 1024 PCI CCD camera as illustrated in *Figure 1*. We measure the height of the objects at x_1 and x_2. The microscope is tilted to provide a side-view with gravity in *(-z)*-direction. We connect the syringes to the microchannel by polyfluoroethylene (PTFE) tubes as shown in *Figure 1* and use two independent syringe pumps (PHD2000, Harvard Apparatus) to drive the sheath flow rate Q_{sheath} and the sample flow rate Q_{sample}. The total flow rate is $Q = Q_{sheath} + Q_{sample}$. In our experiments, the sample flow rate $Q_{sample} = 10\ \mu l/h$ for $Q_{sheath} \leq 240\ \mu l/h$. For higher Q_{sheath} we use $Q_{sample} = 20\ \mu l/h$ to assure sufficient cell influx.

To illustrate the principle of the measurements we demonstrate the separation of RBCs and blood platelets for a moderate flow rate $Q = 200\ \mu l/h$ and a fluid viscosity of $\eta_{out} = 27\ mPas$ in *Figure 1*. After injecting a mixture of RBCs and platelets we measure overlapping height distributions at x_1 with $z_{RBC}(x_1) = (9.5 \pm 1.2)\ \mu m$ and $z_{plat}(x_1) = (10.1 + 2.0)\ \mu m$. Further downstream, at x_2, we observe an increase of RBC height to $z_{RBC}(x_2) = (24.3 \pm 0.5)\ \mu m$ while the blood platelets reach only $z_{plat}(x_2) = (13.3 + 3.2)$ µm. However, RBCs and blood platelets are focused to distinct heights and are clearly separated from each other.

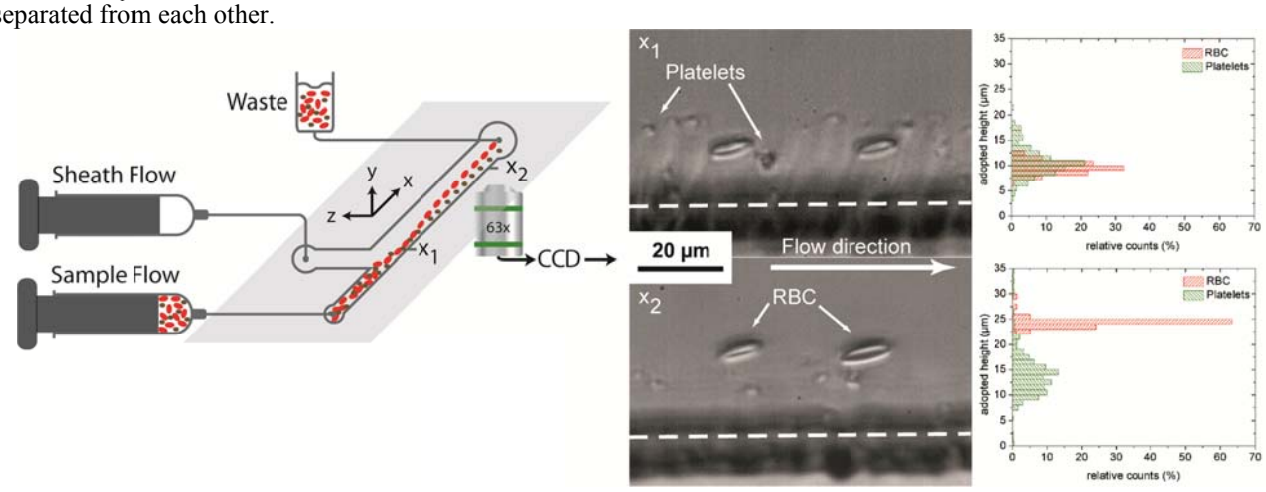

Figure 1: Scheme of the experimental setup and the measurement principle. Q_{sheath} *and* Q_{sample} *are driven by two independent syringe pumps and connected to the PDMS microchannel via PTFE tubes. Videos are recorded and evaluated considering the adopted height of RBCs and blood platelets at the beginning* (x_1) *and the end* (x_2) *of the microchannel. The presented micrographs are recorded at* $Q = 200\mu l/h$ *at* $\eta_{out} = 27mPas$. *The relative counts are determined in intervals of* 1 µm *and a Gaussian curve has been fitted to the histograms to calculate the average height of the objects. Its standard deviation has been identified as a measure for the scattering of the height values.*

RESULTS AND DISCUSSION

We study the effect of shear rate $\dot{\gamma}$ on the separation efficiency in the flow channel. For this purpose, we change the flow rate Q to control the shear rate $\dot{\gamma}$ and observe its effect on the separation efficiency. For a fixed dynamic viscosity $\eta_{out} = 7mPas$, we vary the flow rate from *20 µl/h* to *750 µl/h* and determine the height at x_2 as described above. The adopted heights are shown in *Figure 2(a)*. We observe large initial heights and broad distributions for low sheath flow rates due to the weak hydrodynamic focusing. This is reflected by the final heights and error bars shown in *Figure 2(a)*. At sufficiently strong focusing, the RBCs adopt a constant final height that is independent of Q for flow rates $Q \geq 100\mu l/h$ while platelets and microspheres reach constant heights for slightly higher flow rates of $Q \geq 150\ \mu l/h$. This observation is implied in the theoretical prediction since both, the downstream velocity and the lift velocity scale linear with the flow rate. Thus, the faster lift at higher flow rates is compensated by a shorter transit time of the cells. The enhanced hydrodynamic focusing at higher flow rates yields a better separation and the cell populations are clearly partitioned at $Q = 650\ \mu l/h$ and $Q = 750\ \mu l/h$. We find the adopted heights to be in very good agreement with the theoretical prediction that is represented by the dashed lines in *Figure 2(a)*.

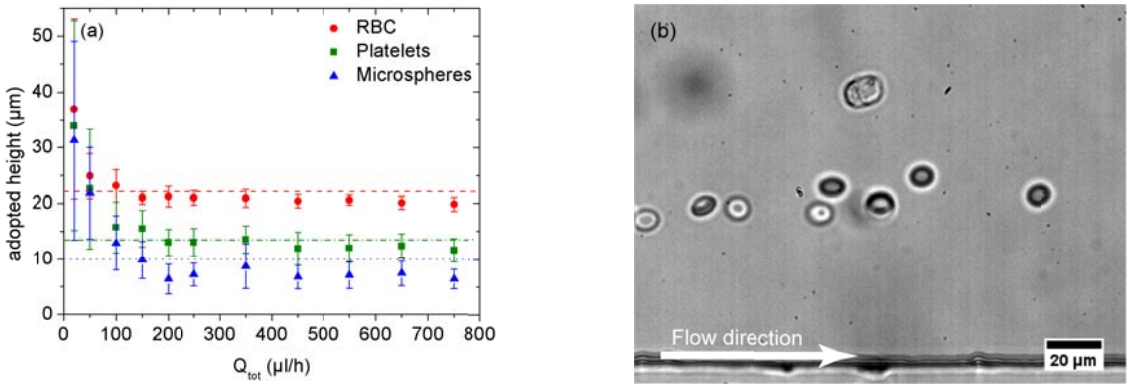

Figure 2: Adopted heights of RBCs, blood platelets and solid microspheres against the flow rate Q at position x_2 and a dynamic viscosity of η_{out} = 7mPas (a). We counted about 250 particles in average per species and data point. The dashed lines represent the results of the calculation with an estimated entrance height of $z(x_1)$ = 10 µm. (b) shows a micrograph of separated MV3-melanoma and red blood cells in the expanded part of the modified microchannel.

For the following experiments with MV3-melanoma cells, we modified the microchannel design to improve the separation process. We reduced the cross section of the main channel to (66 x 63) µm and of the sample inlet to (66 x 30) µm to minimize the broadness of the cell distributions. We expanded the microchannel in z-direction adjacent to x_2 to about four times of its initial height. This leads to a scaling of the adopted heights by the same factor. We measured the adopted heights of the RBCs and the melanoma cells at x_1, x_2 and in the expanded region. For η_{out} = 7mPas and Q = 150 µl/h, the heights of the RBCs are determined as $z_{RBC}(x_1)$ = (13±1) µm, $z_{RBC}(x_2)$ = (16±1) µm and $z_{RBC}(x_{expansion})$ = (60±8) µm. The MV3-cells migrate faster due to their larger diameter of (14±2) µm and adopt the following heights: $z_{MV3}(x_1)$ = (16±1), $z_{MV3}(x_2)$ = (26±4) and $z_{MV3}(x_{expansion})$ = (108±1) µm. These values show the clear separation of the cell populations and the scaling effect of the expansion. The separation is illustrated in *Figure 2(a)*.

CONCLUSION

We demonstrated the separation of RBCs, blood platelets and solid microspheres in a simple microfluidic setup, examined the influence of flow rate on the separation and found very good agreement of our experimental results with the theoretical prediction. Furthermore, we modified the geometry of the microchannel to improve its separation abilities and demonstrated the separation of MV3-melanoma cells from RBCs. In a next step the microchannel will be further modified to enable not only separation but actual sorting of cells in a passive, continuous and label-free manner. The independence of the separation result on flow rate over a large range of flow rates and the simple channel design are advantageous for a potential integration on a microfluidic total analysis system for blood analysis.

ACKNOWLEDGEMENTS

This work was supported by the German Excellence Initiative via NIM, the German Science Foundation (DFG) and the Bavarian Research Foundation (BFS). T. F. thanks Erich Sackmann for helpful discussions. All authors thank Achim Wixforth for his continuous support.

REFERENCES

[1] P. Olla. *J. Phys. II*. 1997, Vol. 7, pp. 1533-1540.
[2] M. Kersaudy-Kerhoas, and E. Sollier. *Lab Chip*. 2013.
[3] A. Karimi, S. Yazdi, and A. M. Ardekani. *Biomicrofluidics*. 2013, Vol. 7, p. 021501 (23).
[4] A. Lenshof, and T. Laurell. *Chem. Soc. Rev*. 2010, Vol. 39, pp. 1203-1217.
[5] P. Olla. *Phys. Rev. Lett*. 1999, Vol. 82, 2, p. 453(4).
[6] C.A. Stan, A. K. Ellerbee, L. Guglielmini, H. A. Stone, G. M. Whitesides. *Lab Chip*. 2013, Vol. 13, pp. 365-376.
[7] A. Farutin, and C. Misbah. *Phys Rev Lett*. 2013, Vol. 110, p. 108104(5).
[8] R. Zhou, and H.-C. Chang. *J. Colloid Interface Sci*. 2005, Vol. 287, pp. 647-656.
[9] R. Zhou, J. Gordon, A. F. Palmer, H.-C. Chang. *Biotechnol. Bioeng*. 2006, Vol. 93, 2, pp. 201-211.
[10] A. Lamura, and G. Gompper. *Europhys. Lett.*. 2013, Vol. 102, p. 28004 (6).
[11] R. Fahraeus, and T. Lindqvist. *Am. J. Physiol*. 1931, Vol. 96, 52, pp. 562-568.
[12] H. Zhao, E. S. G. Shaqfeh, and V. Narsimhan. *Phys. Fluids*. 2012, Vol. 24, p. 011902(21).
[13] M. Abkarian, and A. Viallat. *Biophys. J*. 2005, Vol. 89, pp. 1055-1066.
[14] G. Danker, P. M. Vlahovska, and C. Misbah. *Phys. Rev. Lett*. 2009, Vol. 102, p. 148102(4).
[15] T. M. Geislinger, B. Eggart, S. Braunmüller, L. Schmid, T. Franke. Appl Phys Lett. 2012, Vol. 100, 18, p. 183701(4).

CONTACT

*T. Franke, tel: +49-821-5983312; thomas.franke@physik.uni-augsburg.de